Modeling diffusion limitation in solid-oxide fuel cells

Vinod M. Janardhanan[a,1,2], Olaf Deutschmann[b]

[a] *Department of Chemical Engineering, IIT Hyderabad, Yeddumailaram 502 205, India*
[b] *Karlsruhe Institute of Technology, Engesserstr.20, D-76131 Karlsruhe, Germany*

Abstract

Effect of surface diffusion on the performance of solid-oxide fuel cell is investigated. A methodical approach for the evaluation of surface diffusion coefficients of various adsorbed species based on bond-order conservation Morse potential (BOC-MP) method is presented. The surface diffusion fluxes are used for the evaluation of temporal changes in surface coverages. Our analysis shows that surface diffusion does not lead to the concentration losses in solid oxide fuel cells. Further analysis is carried out and results are presented to substantiate the significance of interface diffusion on the behavior of voltage at limiting current.

Keywords:
Solid-oxide fuel cells; Mathematical modeling;Diffusion limitation;Surface diffusion; Concentration losses; Tortuosity

1. Introduction

Modeling and simulation of solid-oxide fuel cell (SOFC) electrochemical performance is an indispensable task in order to optimize the cell geometry and the cell performance. There is a large body of literature on SOFC modeling starting from zero dimensional models to three dimensional stack models [1, 2, 3, 4]. Majority of these models couple physically based continuum models with Butler-Volmer kinetics for electro-chemistry in-order to predict the cell performance. These mesoscale models consider diffusion laws for finite volume elements [5], which in turn require the micro-structural parameters defining the porous media for the evaluation of effective properties. These properties include the porosity, tortuosity, and the specific area available for surface reactions. The porosity normally rages from 30-40% [6, 7, 8]. The tortuosities of typical modern anode materials are in the rage of 2.0 to 3.5 [9, 8]. However, in SOFC literature anomalously high tortuosities are reported to reproduce the precipitous drop in voltage at limiting current [10, 11]. It is well known in SOFC modeling that an increase in tortuosity or decrease in pore diameter can lead to a precipitous drop in voltage at high current densities. For instance Zhu et al. uses a pore radius of 0.2 μm along with an anode tortuosity of 4.8 to reproduce the experimental observations [12]. Typical pore diameters commonly found in the literature are ∼1 μm [13]. However, in some literature the electrode-pore structures are referred to as macro-pores [14]. Macro-pores typically have diameters greater than 50 nm [15]. An order of magnitude change in the pore radius significantly affects the Knudsen diffusion coefficient since it is directly proportional to the pore radius. Although, the effect of tortuosity on limiting current is well discussed in the literature, influence of pore diameter on limiting current behavior is not well examined. The general trends of limiting current as a function of tortuosities and pore sizes are shown respectively in Fig. 1 and Fig 2.

It is now well established that the high tortuosities are physically unrealistic and are not recommended as a model parameter to reproduce the limiting current behavior. Therefore, there have been few attempts to identify the actual physical process that leads to the limiting current behavior. Notably Williford et al. claimed that the voltage drop at high current density is due to surface diffusion limitations at three-phase boundary (TPB) [9]. In their report Williford et al. claims that for cermets competitive adsorption and coverage dependent surface transport plays a role in the rate limiting behavior. According to them at high current most of the TPB is occupied by H or OH waiting for oxidation by O^{2-} ions. As a result new reactants can not reach the TPBs directly from the gas-phase and surface diffusion becomes rate controlling.

In another report Tsai and Schmidt claims that one must use ”tortuosity factor” instead of tortuosity while calculating the diffusion flux [16]. The tortuosity factor is defined as square of tortuosity. Along the lines of Tsai et al. DeCaluwe et al. follows the proposition by Epstein that finite difference approximations of local gradients of any diffusing property in the porous media should employ the actual path for the differencing distance [17]. Mathematically this is equivalent to using tortuosity factor as proposed by Tsai and Schmidt. Throughout this text whenever there is a reference to tortuosity it is the actual tortuosity and not the tortuosity factor unless otherwise explicitly mentioned.

In a classic report Krishna presented a surface diffusion model that stems from the generalized Maxwell-Stefan equa-

Email address: vj@iith.ac.in (Vinod M. Janardhanan)
[1]Tel: +91-040-2301 6073
[2]Fax: +91-040-2301 6032

tions [18]. This is also the model on which Williford et al. builds up their concentration polarization model. Shi et al. also used the same model to account for surface diffusion effects in an anode supported button cell [19]. According to [18] the occurrence of surface diffusion in parallel with other diffusion mechanisms (Knudsen and molecular) become dominant in the case of micro-pores, which are typically less than 2 nm diameter. However, in SOFC literature pore diameters smaller than 2 nm is rarely reported. Moreover, in the surface diffusion model reported by Krishna the diffusion coefficients are not dependent on the pore-size and hence can not automatically account for surface diffusion flux as a function of pore size distribution. Therefore, the surface diffusion models must be used diligently.

One of the objectives of this work is to assess whether surface diffusion is the actual cause for precipitous drop in voltage at limiting current as claimed by Williford et al. [9]. Shi et al. and Goodwin et al. and Vogler et al. also considered surface diffusion effects in their numerical model [19, 21, 20]. However, Williford et al. and Shi et al. did not solve for the surface coverage explicitly and the surface coverages are estimated from the partial pressures. Moreover, the surface diffusion coefficients are fitted to reproduce the experimental observation based on the a priori assumption that transport of surface adsorbed species leads to the limiting current. Whereas, Vogler et al. solves for the surface coverages and the surface diffusion fluxes are considered for the evaluation of temporal changes in surface coverages. However, they do not account for the coverage dependence of surface diffusion coefficient. The basic difference between our work and Goodwin et al. and Vogler et al. is that Goodwin and Vogler treats a pattern anode and we study porous cermet electrode. Although their work deals with processes that occur close to TPB, the whole approach is still couched up on the principles of mean field approximation. Which in other words mean their treatment like ours is still within the continuum framework. Similar to our approach Vogler and Goodwin does not account for any micro structural changes on a patterned anode. One can expect the presence of kinks and steps on patterned anode surface as well. Vogler et al. claims that adjustments in surface diffusion coefficients were necessary to reproduce the experimental observation, whereas, Goodwin et al. claims that changes in surface diffusion coefficients did not influence the model predictions.

A part of the present work addresses the above gaps in literature. In this work we do not fit the surface diffusion coefficient to reproduce the experimental data, instead we calculate the surface diffusion coefficients from heat of chemisorption data and in turn calculate the surface diffusion fluxes.

2. Theory

2.1. *Surface diffusion*

Modeling surface diffusion process requires reliable estimates for the surface diffusion coefficient $\mathcal{D}_{\mathrm{iV}}$. Defining the total site coverage θ_t as

$$\theta_t = \sum_{i=1}^{N_s} \theta_i = 1 - \theta_V, \tag{1}$$

Vignes relationship gives the generalized Stefan-Maxwell diffusivity (GSM) as [22]

$$\mathcal{D}_{\mathrm{iV}} = (\mathcal{D}^0_{\mathrm{iV}})^{1-\theta_t} (\mathcal{D}^1_{\mathrm{iV}})^{\theta_t}. \tag{2}$$

In the above equations, θ_V is the fraction of the open surface available for adsorption, N_s is the number of adsorbed species on the surface, $\mathcal{D}^0_{\mathrm{iV}}$ is the diffusion coefficient of adsorbed species i on the surface at zero coverage and $\mathcal{D}^1_{\mathrm{iV}}$ is the diffusion coefficient of adsorbed species at full coverage. In the case of single adsorbent the Fick diffusivity is related to GSM according to

$$\mathcal{D}^f_{\mathrm{iV}} = \mathcal{D}_{\mathrm{iV}}/(1-\theta_1). \tag{3}$$

Seebauer and Allen carried out one of the most exhaustive reviews on surface diffusion occurring on metallic substrates and semiconductors [23]. The surface diffusivity $\mathcal{D}$ typically obeys Arrhenius behavior with respect to temperature T:

$$\mathcal{D}_{\mathrm{iV}} = \mathcal{D}_0 \exp(-E_{\mathrm{diff}}/kT). \tag{4}$$

Here, $\mathcal{D}_0$ is the pre-exponential factor, E_{diff} is the activation energy for surface diffusion, T is the temperature, and k is the Boltzmann constant. For metallic substrates D_0 is expected to lie between 10^{-6} and 10^{-7} $\mathrm{m^2 s^{-1}}$ and E_{diff} is related to the desorption energy through the definition of a corrugation ratio

$$\Omega = \frac{E_{\mathrm{diff}}}{E_{\mathrm{des}}}. \tag{5}$$

The histogram of corrugation factor Ω for a large number of adsorbates on metallic substrates yield a Gaussian distribution centered at $\Omega = 0.13$ with a standard deviation of $\sigma = 0.06$. In another interesting work Shustorovich [22] concluded that for mono-atomic adsorbates the activation energy for surface diffusion is related to the heat of chemisorption Q according to

$$E_{\mathrm{diff}} = kQ \quad (0.1 \leq k < 0.3). \tag{6}$$

2.2. *Evaluation of surface diffusion coefficients*

A discussion on surface diffusion will be incomplete without looking in to the mechanistic aspects of electrochemical charge transfer reaction. For H_2 fuel it is assumed that H_2 dissociates into H atoms on the catalytic surface. For Ni cermet anode, this is basically the dissociative adsorption of H_2 on the surface. Since multiple electron charge transfer reactions are rare in nature, it is most likely that the H atom participates in the electrochemical charge transfer reaction. The adsorbed H atom on the Ni surface can react with an OH^- ion on the YSZ to form H_2O, and this H_2O can further dissociatively adsorb on the surface or it can desorb directly into the gas-phase. The dissociative adsorption of H_2O on Ni surface can further lead to the formation of H, OH, or O adsorbed on the surface.

The scenario is more complex when a hydrocarbon fuel is used instead of H_2. For example in the case of CH_4 the possible surface intermediates are H, OH, H_2O, O, CH_4, CH_3, CH_2, CH, CO, CO_2, and HCO. However, the competitive adsorption of certain preferred species makes the surface coverage of all other species almost insignificant. Any diligent discussion on surface diffusion must account for the diffusion of afore mentioned species; especially the preferred ones. However, the bottleneck is the availability of data for the evaluation of surface diffusion coefficients.

In this work bond-order conservation Morse potential (BOC-MP) approach is used for the evaluation of unknown $E_{\text{des}}$for various surface adsorbed species. Couple of examples are discussed here to establish confidence in the evaluation of E_{des} using the heat of chemisorption data Q calculated using BOC-MP method. For mono atomic species E_{diff} can be calculated from Eq. 6. For hydrogen atom adsorbed on Ni(111), the activation energy for surface diffusion is 14.22 kJ mol^{-1} [23]. The heat of chemisorption of H on Ni(111) is 263.5 kJ mol^{-1}, and for k =0.1 Eq. 6 yields the activation energy as 26.3 kJ mol^{-1}. Based on Eq. 6 E_{diff} lies between 26.3 and 79.0 kJ mol^{-1}. The predicted activation energy for surface diffusion in this case exceeds the experimental value by a factor of 1.8. Considering another mono atomic system, O on Pt(111), the experimentally observed value of activation energy for surface diffusion, E_{diff} is 113 kJ mol^{-1}. The heat of chemisorption of O on Pt(111) is 355 kJ mol^{-1}, and Eq. 6 with k=0.3 yields E_{diff} = 106.6 kJ mol^{-1}, in close agreement with experimentally observed value.

For diatomic adsorbates the desorption energy E_{des} is same as the heat of chemisorption Q. For example the heat of chemisorption Q of CO on Ni(111) is 121 kJ mol^{-1} [24], and experimentally found E_{des} is 108 kJ mol^{-1} [23]. Similarly for CO on Pt(111) Q is 133.8 kJ mol^{-1} and E_{des} is also 133.8 kJ mol^{-1}. Another example of diatomic system is NO on Pt(111); the heat of chemisorption Q is 108.7 kJ mol^{-1} and the desorption energy E_{des} is 124.6 kJ mol^{-1}, all in close agreement with experimentally observed values. Therefore, we can confidently assume that the desorption energy is same as the heat of chemisorption and by knowing E_{des} the activation energy for E_{diff} can be calculated from Eq. 5.

Extensive data is not available for the comparison of polyatomic adsorbates. Based on the limited data we can make the following observations. For NH_3 on Re(100) E_{des} is 83.6 kJ mol^{-1}, in good agreement with BOC-MP prediction of 86.0 kJ mol^{-1} as the heat of chemisorption Q. For CH_4 on Pt(111) the BOC-MP predicted heat of chemisorption is 25 kJ mol^{-1} and E_{des} is 15.0 kJ mol^{-1}. Therefore, we treat polyatomic adsorbates in the same manner as diatomic adsorbates. From the above discussion it is clear that we can confidently use BOC-MP method to calculate E_{des}. For small activation barriers the discrepancy is less than a factor of 2. Moreover, we have reliable estimates for all the major surface adsorbed species. Table 1 lists the data required for the evaluation of $\mathcal{D}^0_{\text{iV}}$. A parity plot for the calculated and the experimental observations for E_{diff} is shown in Fig. 3. Generally the surface diffusion coefficient at full coverage is much lower than the one at zero coverage [18]. Therefore, for brevity sake we assume

$$\mathcal{D}^1_{\text{iV}} = 0.1 \times \mathcal{D}^0_{\text{iV}}. \tag{7}$$

2.3. *SOFC button cell model*

Performance modeling of SOFC requires to resolve the coupled interactions between porous media transport, heterogeneous chemistry, and electrochemistry. The species transport in one dimension along the thickness of the porous electrodes is modeled according to

$$\frac{\partial(\epsilon\rho Y_k)}{\partial t} = -\frac{\partial j_k}{\partial y} + A_s W_k \dot{s}_k, \tag{8}$$

and the density of the mixture according to

$$\frac{\partial(\epsilon\rho)}{\partial t} = -\sum_{k=1}^{N_g} \frac{\partial j_k}{\partial y} + \sum_{k=1}^{N_g} A_s W_k \dot{s}_k \tag{9}$$

In the above equations, ϵ is the porosity, ρ is the density, Y_k is the mass fraction of species k, t is the time, j_k is the mass flux of species k, y is the independent coordinate, A_s is the specific area, W_k is the molecular weight of species k, $\dot{s}_k$ is the molar production rate of species k, and N_g is the number of gasphase species. The species flux j_k within the porous media is calculated using dusty gas model [25]. Dusty gas model is an implicit relationship among molar concentrations, concentration gradients, pressure gradient, binary diffusion coefficients, and Knudsen diffusion coefficients. The molar flux according to dusty gas model is written as

$$J_k = -\sum_{l=1}^{N_g} \mathcal{D}^{\text{DGM}}_{kl} \nabla[X_l] - \left[\sum_{l=1}^{N_g} \mathcal{D}^{\text{DGM}}_{kl} \frac{[X_l]}{\mathcal{D}^e_{l,Kn}}\right] \frac{B_g}{\mu} \nabla p, \tag{10}$$

where $[X_l]$ is the molar concentration of species l, B_g is the permeability, μ is the viscosity, p is the pressure, $\mathcal{D}^e_{l,Kn}$ is the effective Knudsen diffusion coefficient, and $\mathcal{D}^{\text{DGM}}_{kl}$ is the DGM diffusion coefficients. The permeability is calculated according to Kozeny-Carman relationship:

$$B_g = \frac{\epsilon^3 d_p^2}{72\tau_g(1-\epsilon)^2}, \tag{11}$$

where, τ is the tortuosity and d_p is the particle diameter. The DGM diffusion coefficients is defined as a matrix inverse

$$\mathcal{D}^{\text{DGM}}_{kl} = \mathcal{H}^{-1}, \tag{12}$$

where the elements of $\mathcal{H}$ matrix are

$$h_{kl} = \left[\frac{1}{\mathcal{D}^e_{k,Kn}} + \sum_{j\neq k} \frac{X_j}{\mathcal{D}^e_{kj}}\right]\delta_{kl} + (\delta_{kl} - 1)\frac{X_k}{\mathcal{D}^e_{kl}}. \tag{13}$$

In this expression X_k are mole fractions, δ_{ij} is the Kronecker delta, and $\mathcal{D}^e_{kl}$ is the effective binary diffusion coefficient. The pressure p within the porous media is calculated according to the ideal gas equation

$$p\bar{M} = \rho RT, \tag{14}$$

where $\bar{M}$ is the average molecular weight. Solution of Eq. 8 and Eq. 9 requires the reaction source terms $\dot{s}_k$ and boundary conditions at the electrode-gas chamber interfaces (open electrode surface) and electrode-electrolyte interfaces. At the electrode-gas chamber interface the inlet mass fractions serve as boundary condition and at the electrode-electrolyte interface the species fluxes are zero. The electrochemical reaction source terms for electrochemically active species are calculated from the current density and is accounted along with the chemical source terms. The evaluation of current density and the reaction source terms are respectively explained in the following sections for electrochemistry and heterogeneous chemistry.

2.4. *Electrochemical model*

A distributed charge transfer model is implemented to assess the impact of surface diffusion. The charge conservation equations used in the distributed charge transfer model are based on continuum conservation equations; representing the transport of electrons in the electron conducting phase of the membrane electrode assembly (MEA) and ion transport in the ion conducting phase of MEA. The electrode facilitates the transport of both ions as well as electrons, whereas the dense electrolyte facilitates only the transfer of ions. When electrical load is applied to the cell, the electrode and the electrolyte phase develops characteristic potential profiles and the electrochemical reactions depend on the local potential difference between the electronic and ionic phases. The conservation of charges within the MEA can be formulated based on Ohms law [26, 27, 19, 14]. Under steady state conditions the charge conservation for electron conducting phase and ion conducting phase is written as

$$\frac{d}{dy}\left(\sigma^{\mathrm{e}}_{\mathrm{m}}\frac{\varphi_{\mathrm{m}}}{dy}\right) = \pm i. \tag{15}$$

Here, $\sigma^{\mathrm{e}}_{\mathrm{m}}$ is the effective conductivity and φ_{m} is the potential of phase m in the composite electrode, i is the current, and y is the independent coordinate. The choice of sign in Eq. 15 depends on the particular phase in the composite electrode. The effective conductivities are evaluated using simple Bruggmann correlation [28]

$$\sigma^{\mathrm{e}}_{\mathrm{m}} = \phi^{3/2}_{\mathrm{m}}\sigma_{\mathrm{m}}. \tag{16}$$

Here, ϕ_{m} is the volume fraction of the conductive phase m and σ_{m} is the pure phase conductivity. The electronic conductivity in the anode and cathode is evaluated as a function of temperature according to

$$\sigma_{\mathrm{anode}} = 3.27 \times 10^4 - 10.653T \tag{17}$$

and

$$\sigma_{\mathrm{cathode}} = \frac{8.855 \times 10^5}{T}\exp\left(\frac{-9000}{RT}\right). \tag{18}$$

The pure phase conductivity for the electrolyte phase is taken from [25].

The measured cell potential is given by the difference in electronic potentials of the current collectors at the cathode and the anode. Assuming uniform potential throughout the current collectors, the cell voltage can be expressed as

$$E_{\mathrm{cell}} = \varphi_{\mathrm{c}} - \varphi_{\mathrm{a}}. \tag{19}$$

Here, φ_{c} and φ_{a} are respectively the electronic potentials at the cathode and anode current collectors. Generally there is a spacial variation of the electrode potentials along the thickness of the composite electrodes due to double layer formation. Solution of Eq. 19 requires boundary condition at the respective domains. Since the transport of ions is continuous throughout the MEA structure, boundary conditions are required only at the current collectors. The current collectors are pure electronic conductors and therefore, the ion flux φ_{io} vanish at the current collectors leading to

$$\frac{d\varphi_{\mathrm{io}}}{dy} = 0. \tag{20}$$

Since the dense electrolyte is a pure ion conductor, unlike ion transport, electron transport is not continuous throughout MEA. Therefore, for the electrode phase potential four boundary conditions are required; for each current collectors and at the electrode dense electrolyte interfaces. Since the electron flux φ_{el} vanishes at the dense electrolyte electrode interface

$$\frac{d\varphi_{\mathrm{el}}}{dy} = 0. \tag{21}$$

We arbitrarily set the electrode potential at the cathode current collector to zero, which automatically sets the potential of the anode current collector according to Eq. 19. A schematic of the implementation of various boundary conditions are shown in Fig. 4.

Using the Butler-Volmer formalism presented in Zhu et al. [25], the electrochemical charge transfer at the anode is evaluated according to

$$i = i_0\left[\exp\left(\frac{(1+\beta_a)F\eta_{\mathrm{a}}}{RT}\right) - \exp\left(\frac{-\beta_a F\eta_{\mathrm{a}}}{RT}\right)\right] \quad , \tag{22}$$

and for cathodic charge transfer reactions according to

$$i = i_0\left[\exp\left(\frac{\beta_c F\eta_{\mathrm{c}}}{RT}\right) - \exp\left(\frac{-(1-\beta_c)F\eta_{\mathrm{c}}}{RT}\right)\right]. \tag{23}$$

In the above equations, β is the charge transfer coefficients, F is the Faraday constant, i_0 is the volumetric exchange current density, and η is the local activation overpotentials in the composite electrodes. The local over potential is defined as

$$\eta = \varphi_{\mathrm{el}} - \varphi_{\mathrm{io}} - E_{\mathrm{ref}}, \tag{24}$$

where E_{ref} is the relative potential difference between the electronic and ionic conductors at reference state. By setting the reference state for anode activation overpotential to zero, the reference state for the cathode overpotential becomes the open circuit potential [19]. i.e the above equation can be respectively written for the anode and cathode as

$$\eta_{\text{a}} = \varphi_{\text{el}} - \varphi_{\text{io}} \tag{25}$$

and

$$\eta_{\text{c}} = \varphi_{\text{el}} - \varphi_{\text{io}} - E_{\text{rev}}. \tag{26}$$

Here E_{rev} is the reversible potential. The exchange current density for the anode side charge transfer reaction is expressed as function of open surface and surface coverages of hydrogen according to

$$i_0 = i_a^* \theta_{\text{H}}(1 - \theta_t), \tag{27}$$

so that changes in surface coverage due to surface diffusion affects the resulting current density.

For the cathode, exchange current density is evaluated according to [25]

$$i_0 = i_c^* \frac{(p_{\text{O}_2}/p_{\text{O}_2}^*)^{1/4}}{1 + (p_{\text{O}_2}/p_{\text{O}_2}^*)^{1/2}}. \tag{28}$$

In the above equations i_a^* and i_c^* are empirically fitted parameters, and p_{O_2} is the partial pressure of oxygen. $p_{\text{O}_2}^*$ is expressed in the Arrhenius form according to [25].

2.5. *Heterogeneous chemistry*

The net molar production rate $\dot{s}_k$ of a gaseous or surface adsorbed species due to heterogeneous reaction is given by

$$\dot{s}_k = \sum_{i=1}^{R_s} \nu_{ki} k_{fi} \prod_{k=1}^{N_g+N_s} [X_k]^{\nu\prime_{ki}}. \tag{29}$$

Here R_s is the number of surface reactions, N_g and N_s respectively represents the number of gas phase species and surface species, $[X_k]$ is the concentration of species k, k_{fi} is the forward rate constant for reaction i, and ν_{ki} is the difference in stoichiometric coefficient for species k between the products and reactants in reaction i. $[X_k]$ will have the unit of mol m^{-3} for gas phase species and mol m^{-2} for surface species.

Based on mean field approximation the forward rate constant is expressed in the Arrhenius form for i'th chemical reaction as

$$k_{fi} = A_i T^{\beta} \exp\left(-\frac{E_{ai}}{RT}\right) \prod_{k=1}^{N_s} \theta_k^{\mu_{ki}} \exp\left(-\frac{\epsilon_{ki}\theta_k}{RT}\right). \tag{30}$$

Here A_i is the pre-exponential, E_{ai} is the activation energy, μ is the order dependency, θ is the surface coverage, β is the temperature exponent, R the gas constant, T the temperature, and ϵ is the coverage dependent activation energy. The surface coverage θ is related to the surface concentration according to

$$\theta_k = \frac{[X_k]\sigma_k}{\Gamma}. \tag{31}$$

In the above equation σ_k is the site occupancy number and Γ is the total site density in mol m^{-2}. The heterogeneous chemical reaction mechanism used in this work is taken from [29]. The temporal changes in surface coverages are calculated according to

$$\frac{\partial \theta_k}{\partial t} = -\frac{\partial}{\partial y}\mathcal{J}_k + \frac{\sigma_k}{\Gamma}\dot{s}_k, \quad k = 1 \ldots N_s. \tag{32}$$

Here $\mathcal{J}_k$ and $\dot{s}_k$ are respectively the surface diffusion flux and surface production rate of species k, and N_s is the number of surface adsorbed species. For any further information on modeling heterogeneous chemistry the reader is referred to [30].

On a continuum scale the total surface flux $\mathcal{J}_k$ is expected to depend on the tortuosity of surface diffusion path and the availability of percolating surfaces. At molecular level the transferring species never leaves the force field exerted by the surface [18]. Therefore, one has to consider the actual diffusing path instead of the straight line difference. Assuming that the average length of percolating surface is at-least equal to the finite volume cell thickness, and by introducing an effectiveness factor based on porosity and tortuosity, the surface diffusion flux is calculated according to Fick's law:

$$\mathcal{J}_k = -\frac{\epsilon}{\tau}\mathcal{D}_{kV}\frac{d\theta_k}{dy}. \tag{33}$$

However, the sum of fluxes of all mobile atoms on the surface must be zero [18] and the nickel particle themselves are mobile at the temperature considered in this work. Therefore, to ensure the conservation of fluxes the flux of Ni is calculated according to

$$\mathcal{J}_{\text{Ni}} = -\sum_{k=1,k\neq Ni}^{N_s} \mathcal{J}_k \tag{34}$$

3. Results and discussion

As discussed in the previous sections, implementation of surface diffusion into any transport model requires accurate estimates of surface diffusion coefficients at least for the major surface adsorbed species. Our calculations show that in the case of H_2 fuel the major surface adsorbed species is H and most of the surface remains open. Figure 5 shows the surface coverages of the adsorbed species and the open Ni surface. Figure 6 shows the case of CH_4 fuel, where majority of the surface is occupied by CO and H and most of the surface remains open for adsorption by other species.

To assess the influence of surface diffusion fluxes, we carried out simulations with and without surface diffusion model. Figure 7 shows the surface diffusion flux of major surface adsorbed species for 70% H_2 and 30% H_2O at E_{cell} = 0 V and E_{cell} =0.7 V. The parameters used for the simulation are given in Table 2. The magnitude of these fluxes are too low to cause any significant changes in the surface coverage profile.

In fact we observe that the surface coverages are same for both cases upto three decimal places. When the surface fluxes can not alter the surface coverages significantly, the volumetric current density will remain the same for both cases. It has to be observed that we use a $\mathcal{D}_0$ value of 10^{-6} m^2s^{-1}, which is on the higher side of the range proposed by Seebuer et al. for $\mathcal{D}_0$. Therefore, the fluxes reported in Fig. 7 are the maximum possible under the current modeling framework. The resulting ionic and electronic current densities at 0.7 V are shown in Fig. 8. Since there is no significant influence of surface diffusion (even at limiting current) the curves for cases with and without surface diffusion overlap each other. The same behavior is observed at zero potential and hence it is not shown in the figure.

Having demonstrated that surface diffusion does not influence the limiting current behavior, our next objective is to find out the actual cause for the behavior at limiting current. For the discussions which follow we do not use the distributed charge transfer model presented in section 2.3 any more, instead we use the electrochemistry model described by Zhu et al. [25]. The exchange current densities are calculated using the composition at the dense electrolyte-electrode interface according to [25], which requires two adjustable parameters $i^*_{H_2}$ and $i^*_{O_2}$. The distributed charge transfer model is used only for the assessment of surface diffusion effects.

Most of the button cell models assume that the concentration at the electrode-gas chamber interface is same as that of the inlet composition. In reality the composition at the electrode-gas chamber interface is different from the inlet composition due to back diffusion of the products, especially when the inlet flow rates are low. We have previously studied these effects in 2D using Fluent software and the composition of H_2 in the anode compartment for an inlet fuel mixture containing 97% CH_4 and 3% H_2O is shown in Fig. 9 [31]. It is evident from the figure that the composition at the anode-fuel chamber interface is different from the inlet composition due to back diffusion of the products which dilutes the fuel composition at the anode-gas chamber interface. These 2D calculations are not a part of this work and is adapted from [31]

One-dimensional button cell models do not generally account for the inlet tube and the computational domain consists only the membrane electrode assembly (MEA). Therefore, the back diffusion of the product species must be accounted for in the boundary condition used at the electrode-gas chamber interface. There have been a few works in this direction [32, 33, 12]. Bessler in his work [32] models the spacial variation in gas phase composition above the electrode surface, but does not consider the porous media transport. Primmdahl et al. and Zhu et al uses a continuous stirred tank reactor model to simulate the gas chamber above the electrodes. Different from the above mentioned works, we use a simple flux continuity boundary condition at the electrode-gas chamber interface to resolve the back diffusion. i.e,

$$Y_{k,\text{in}} - Y_{k,\text{interface}} + \frac{j_k}{\dot{m}} = 0. \tag{35}$$

Here $Y_{k,\text{in}}$ is the mass fraction inlet fuel and $Y_{k,\text{interface}}$ is the mass fraction at the electrode-gas chamber interface, j_k is the mass flux of species k at the interface, and $\dot{m}$ is the inlet flow rate. In fuel cell literature the commonly employed boundary condition is

$$Y_{k,\text{in}} = Y_{k,\text{interface}}. \tag{36}$$

This boundary condition will fix the electrode-gas chamber interface species mass fractions at the inlet mass fraction, and will not allow for back diffusion. On the other hand Eq. 35 will let the species mass fractions at the electrode-gas chamber interface to change according to the mass flux at the interface which are calculated according to the dusty gas model (Eq. 10). Eq. 35 is solved together with Eqs. 8, 9, and 14.

Figure 10 shows the effect of inlet velocity on the behavior at limiting current. A decreasing inlet velocity leads to trends similar to that of increasing tortuosity. Comparison of experimental data and models predictions for the data reported by Shi et al. [19] is shown in Fig. 11. Shi et al. in their modeling study used a tortuosity value of 14 to reproduce the experimental data for 20% H_2 and 80% H_2O without accounting for the local composition. All the parameters used to reproduce the experimental data are taken from [19] except the tortuosity. For the calculations presented in Fig. 11 a tortuosity value of 3.5 is used. Leakage over potential is considered as described by Zhu et al.[25], i.e

$$\eta_{\text{leak}} = \eta_{\max}(1 - \frac{i}{i_{\max}}). \tag{37}$$

We use $\eta_{\text{leak}} = 0.05$ V and $i_{\max} = 8.0$ A cm^{-2} to reproduce the open circuit potentials. The velocity at air and fuel side is kept at 5 ms^{-1} and 0.05 ms^{-1} respectively. The whole set of parameters used for the results presented in Fig. 11 are given in Table 3. Without making use of high tortuosity values as high as 14, the model predictions are in good agreement with experimental data just by implementing a flux continuity boundary condition.

4. Conclusions

Using heat of chemisorption data for various surface adsorbed species calculated using BOC-MP method we have calculated the surface diffusion fluxes, and the temporal changes in surface coverage are calculated by accounting for the surface diffusion fluxes. Our calculations show that surface diffusion fluxes do not lead to the precipitous drop in cell voltage at limiting current. By implementing flux continuity boundary condition we demonstrated that the limiting current behavior can originate from the back diffusion of the product species which alters the fuel composition at the electrode-gas chamber interface. The back diffusion is more pronounced at low approach velocities. In fact a decrease in approach velocity is similar in

effect to increasing the tortuosity value. Therefore, any button cell modeling effort must account for the interface diffusion to get reliable estimates of unknown parameters. Therefore, SOFC button cell models must account for inlet flow rate in order to estimate model parameters that are with in the physically realistic range and reliable.

[1] S.H. Chan, K.A. Khor, Z.T. Xia, J. Power Sources 93 (2001) 130.
[2] A.C. Burt, I.B. Celik, R.S. Gemmen, A.V. Smirnov, J. Power Sources 126 (2004) 76.
[3] B.A. Haberman, J.B. Young, Int. J. Heat Mass Transfer 47 (2004) 3617.
[4] N. Autissier, D. Larrain, J. Van, D. Favrat, J. Power Sources 131 (2004) 313.
[5] E.I. Tiffée, A. Weber, K. Schmid, V. Krebs, Solid State Ionics 174 (2004) 223.
[6] J. Divisek, R. Wilkenhöner, Y. Volfkovich, J. Appl. Electrochem. 29 (1999) 153.
[7] D. Gostovic, J.R. Smith, D.P. Kundinger, K.S. Jones, E.D. Wachsman, Electrochem. Solid-State Lett. 10 (2007) B2007.
[8] J.R. Wilson, W. Kobsiriphat, R. Mendoza, H.Y. Chen, J. M. Hiller, D.J. Miller, K. Thornton, P.W. Voorhees, S.B. Adler, S.A. Barnett, Nat. Mater. 5 (2006) 541.
[9] R.E. Williford, L.A. Chick, G.D. Maupin, S.P. Simner, J.W. Stevenson, J. Electrochem. Soc. 150 (2003) A1067.
[10] J.W. Kim, A.V. Virkar, K.Z. Fung, K. Mehta, S.C. Singhal, J. Electrochem. Soc. 146 (1999) 69.
[11] P. Costamagna, K. Honegger, J. Electrochem. Soc. 145 (1998) 3995.
[12] H. Zhu, R.J. Kee, J. Electrochem. Soc. 153 (2006) A1765.
[13] D. Simwonis, F. Tietz, D. Stover, Solid State Ionics 132 (2000) 241.
[14] P. Costamagna, P. Costa, V. Antonucci, Electrochim. Acta 43 (1998) 375.
[15] R. Krishna, Chem. Eng. Sci. 48 (1993) 845.
[16] C.l. Tsai, V.H. Schmidt, J. Power Sources 196 (2011) 692.
[17] S.C. Decaluwe, H. Zhu, R.J. Kee, G.S. Jackson, J. Electrochem. Soc. l55 (2008) B538.
[18] R. Krishna, Chem. Eng. Sci. 45 (1990) 1779.
[19] Y. Shi, N. Cai, C. Li, J. Power Sources 164 (2007) 639.
[20] M. Vogler, A. Bieberle-hütter, L. Gauckler, J. Warnatz, W.G. Bessler, J. Electrochem. Soc. 156 (2009) B663.
[21] D.G. Goodwin, H. Zhu, A.M. Colclasure, R.J. Kee, J. Electrochem. Soc. 156 (2009) B1004.
[22] E. Shustorovich, J. Am. Chem. Soc. 106 (1984) 6479.
[23] E.G. Seebauer, C.E. Allen, Prog. Surf. Sci. 49 (1995) 265.
[24] E. Shustorovich, Adv. Catal. 37 (1990) 101.
[25] H. Zhu, R.J. Kee, V.M. Janardhanan, O. Deutschmann, D.G. Goodwin, J. Electrochem. Soc. 152 (2005) A2427.
[26] H. Zhu, R.J. Kee, J. Electrochem. Soc. 155 (2008) B715.
[27] S. Sunde, J. Electroceramics 5 (2000) 153.
[28] B. Kenney, K. Karan, Proc. Hydrogen and Fuel Cells Conference and Trade Show, Toronto, Canada, Sept. (2004)
[29] V.M. Janardhanan, O. Deutschmann, J. Power Sources 162 (2006) 1192.
[30] R.J. Kee, M.E. Coltrin, P. Glarborg, Chemically reacting flow: Theory and Practice, 1st ed., John Wiley & Sons, Hoboken, NJ, 2003.
[31] V.M. Janardhanan, A detailed approach to model transport, heterogeneous chemistry, and electrochemistry in solid-oxide fuel cells, Ph.D. thesis, KIT 2007
[32] W.G. Bessler, J. Electrochem. Soc. 153 (2006) A1492.
[33] S. Primdahl, M. Mogensen, J. Electrochem. Soc. 145 (1998) 2431.

Table 1: Surface diffusion coefficients at zero coverage

System	D_0 (m^2s^{-1})	Q kJ mol^{-1}	Ω	k	E_{diff} (kJ mol^{-1})	Ref
CH_4/Ni(111)	10^{-6}	25.1	0.14	-	3.51	BOC-MP
CH_3/Ni(111)	10^{-6}	200.8	0.14	-	28.11	BOC-MP
CH_2/Ni(111)	10^{-6}	347.2	0.14	-	48.61	BOC-MP
CH/Ni(111)	10^{-6}	485.3	0.14	-	67.94	BOC-MP
CO_2/Ni(111)	10^{-6}	25.1	0.14	-	3.51	BOC-MP
H_2O/Ni(111)	10^{-6}	71.1	0.14	-	9.95	BOC-MP
HCO/Ni(111)	10^{-6}	209.2	0.14	-	29.28	BOC-MP
OH/Ni(111)	10^{-6}	255.2	0.14	-	35.73	BOC-MP
CO/Ni(111)	10^{-7}	-	-	-	28.45	[23]
O/Ni(111)	10^{-6}	481.1	-	0.3	144.34	BOC-MP [22]
C/Ni(111)	10^{-6}	715.5	-	0.3	214.63	BOC-MP [22]
H/Ni(111)	10^{-6}	-	-	-	14.22	[23]

Table 2: Parameter values used for distributed charge transfer model with surface diffusion.

Parameter	Anode	Electrolyte	Cathode
Thickness (μm)	100	25	30
Porosity	35%	-	35%
Tortuosity	3.8	-	3.8
Pore diameter (μ m)	1.0	-	1.0
Particle diameter (μm)	2.5	-	2.5
Volume fraction, ϕ	23%	-	31%
Specific area (m^{-1})	1025×10^2	-	-
i^* (A cm^{-3})	8.5×10^3	-	2.8×10^3
Conductivity (S cm^{-1})	3.27×10^4 - 10.653 T	$\frac{3.6\times10^5}{T}\exp\left(\frac{-8\times10^4}{RT}\right)$	$\frac{8.855\times10^5}{T}\exp\left(\frac{-9000}{RT}\right)$

Table 3: Parameter values used for reproducing experimental results in [19]

Parameter	Anode	Electrolyte	Cathode
Thickness (μm)	1100	10	60
Porosity	35%	-	35%
Tortuosity	3.8	-	3.8
Pore diameter (μ m)	1.0	-	1.0
Particle diameter (μm)	2.5	-	2.5
i^* (A cm^{-2})	8.5	-	2.8
Velocity (m/s)	0.05	-	5
Leakage overpotential, η_{max}, (V)	-	0.05	-
Leakage overpotential, i_{max}(A cm^{-2})	-	8	-
Ionic conductivity (S cm^{-1})	-	(3.6×10^5/T) exp(-8.0×10^4/RT)	-

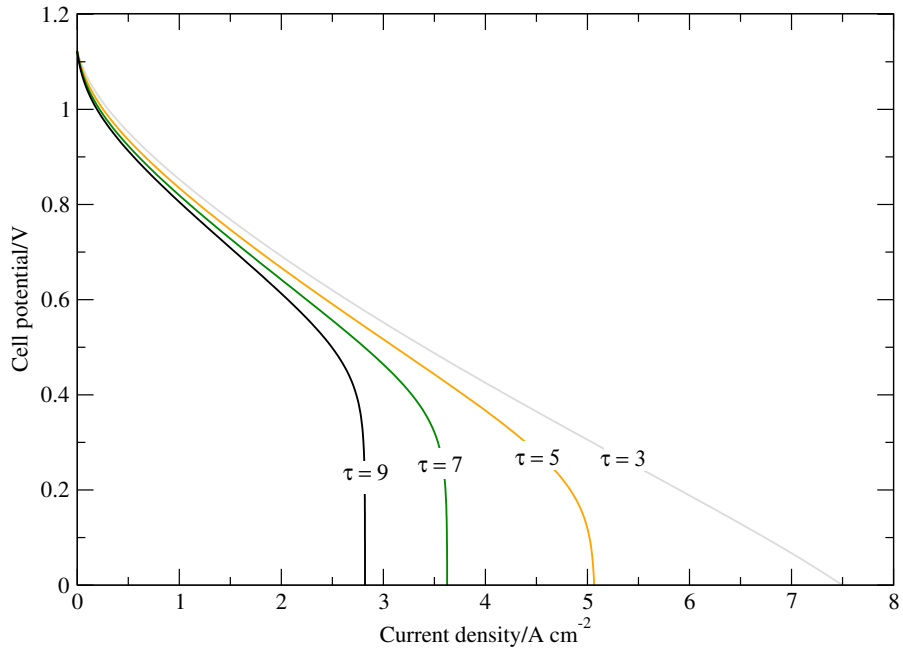

Figure 1: Effect of tortuosity on the behavior of limiting current. (*Note: τ is the tortuosity not the tortuosity factor.*

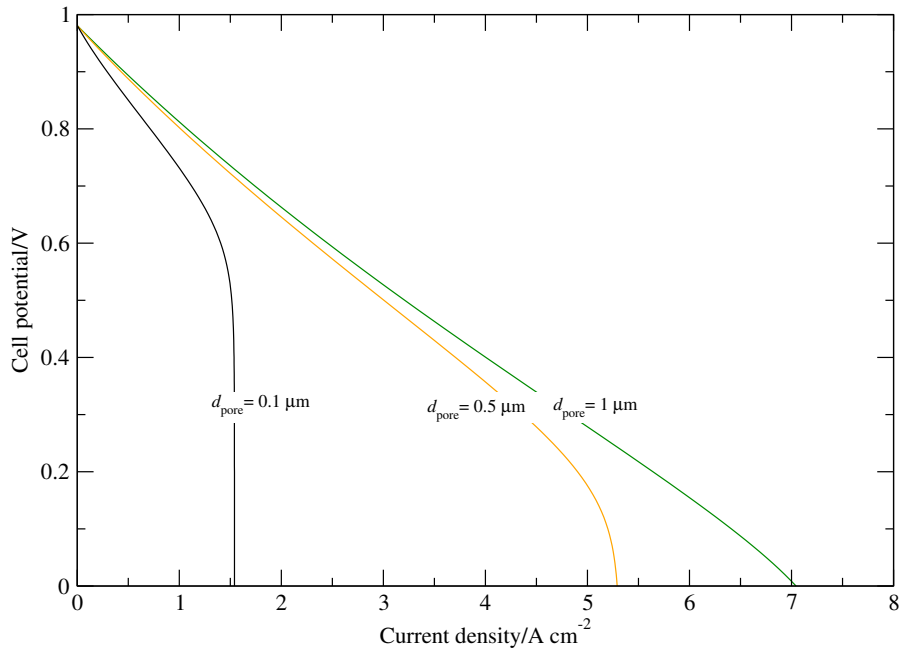

Figure 2: Effect of pore size on the behavior of limiting current.

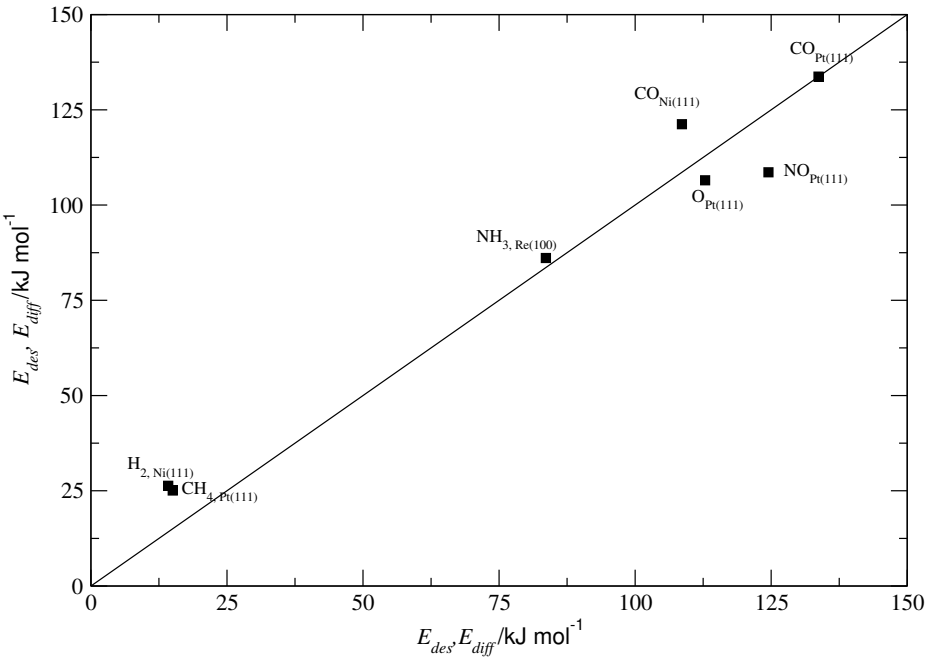

Figure 3: Parity plot for the calculated and experimentally observed desorption energy or activation energy for surface diffusion. *Y* axis represents the theoretical predictions and *X* axis represents the experimental observations.

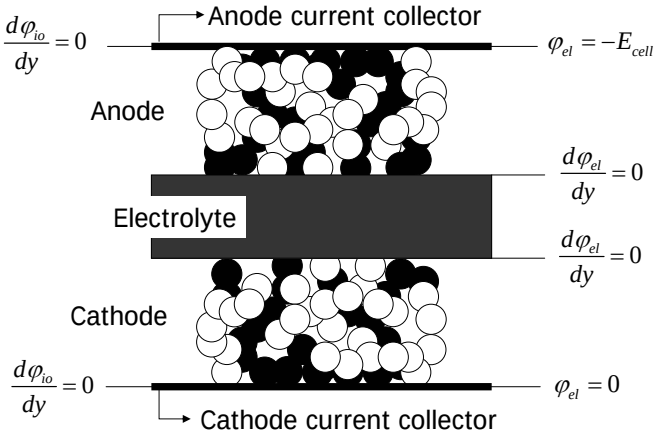

Figure 4: A schematic of the boundary conditions for the calculation of ionic and electronic fluxes for the distributed charge transfer model.

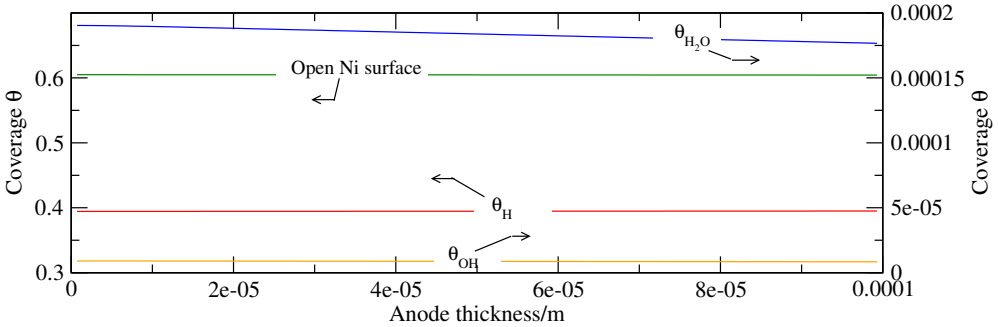

Figure 5: Surface coverages of various surface adsorbed species for H_2 fuel. 70% H_2 diluted in steam is assumed to enter the cell, T = 1073 K, E_{cell} = 0.7 V.

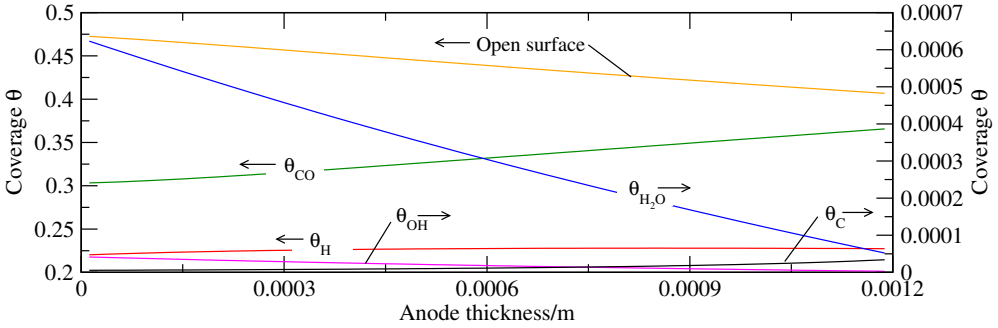

Figure 6: Surface coverages of various surface adsorbed species for a fuel mixture of 10% CH_4, 66% H_2, 20%CO, and 4% H_2O, T= 1073 K, E_{cell} = 0.7 V.

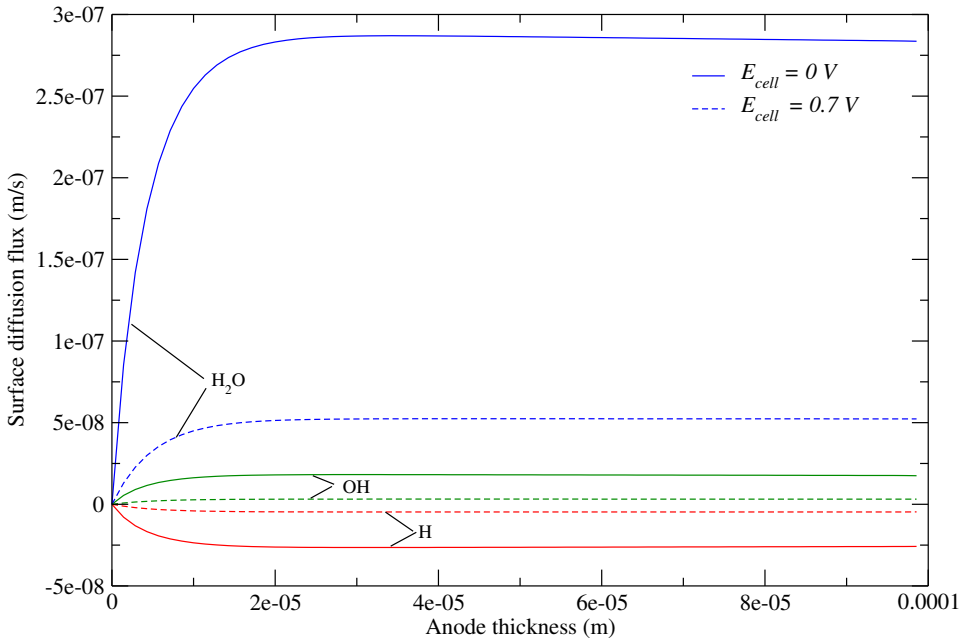

Figure 7: Surface diffusion flux of various surface adsorbed species for 70% H_2 diluted in H_2O.

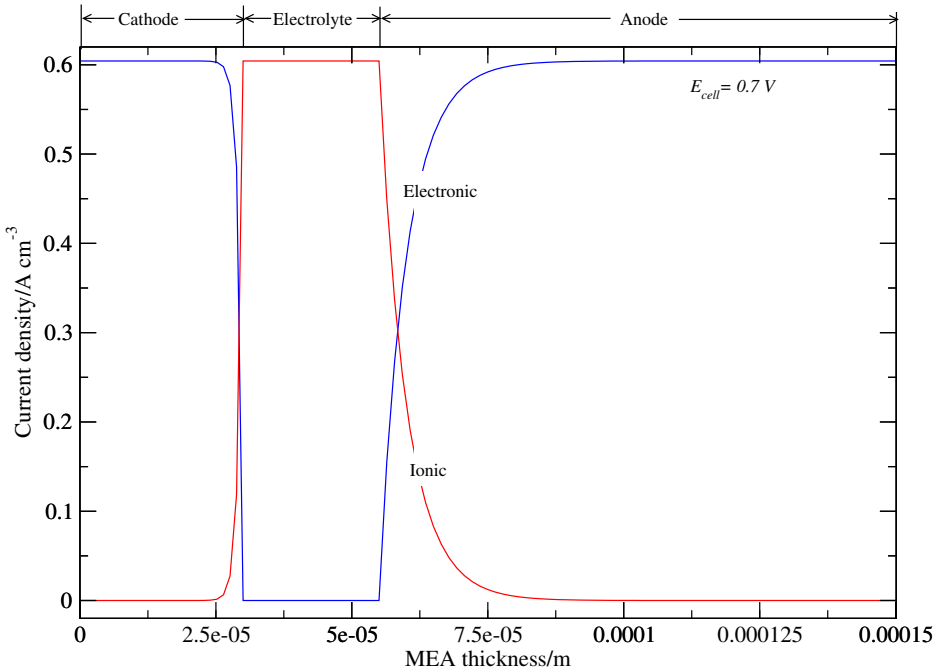

Figure 8: Distribution of ionic and electronic current for a case with and without surface diffusion. Since surface diffusion does not contribute anything both the curves overlap.

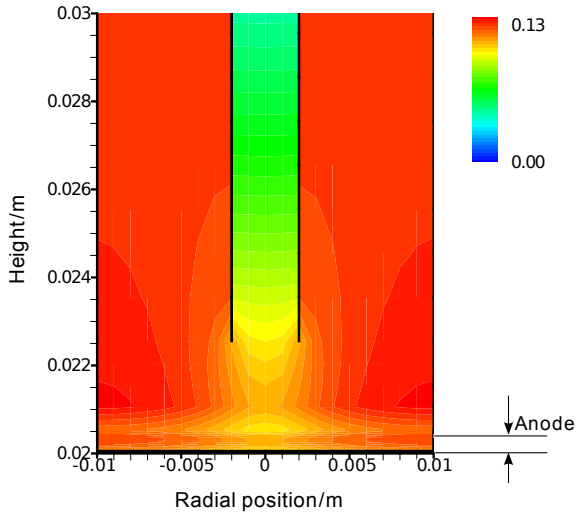

Figure 9: Contours of H_2 mole fraction for an inlet mixture containing 97% CH_4 and 3% H_2O.

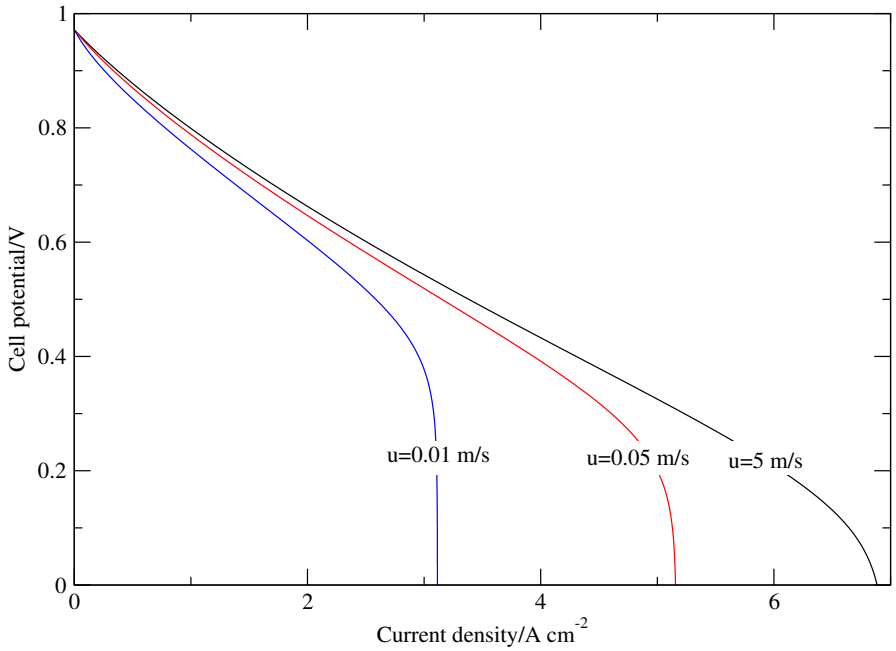

Figure 10: Effect of inlet fuel velocity on the behavior of limiting current.

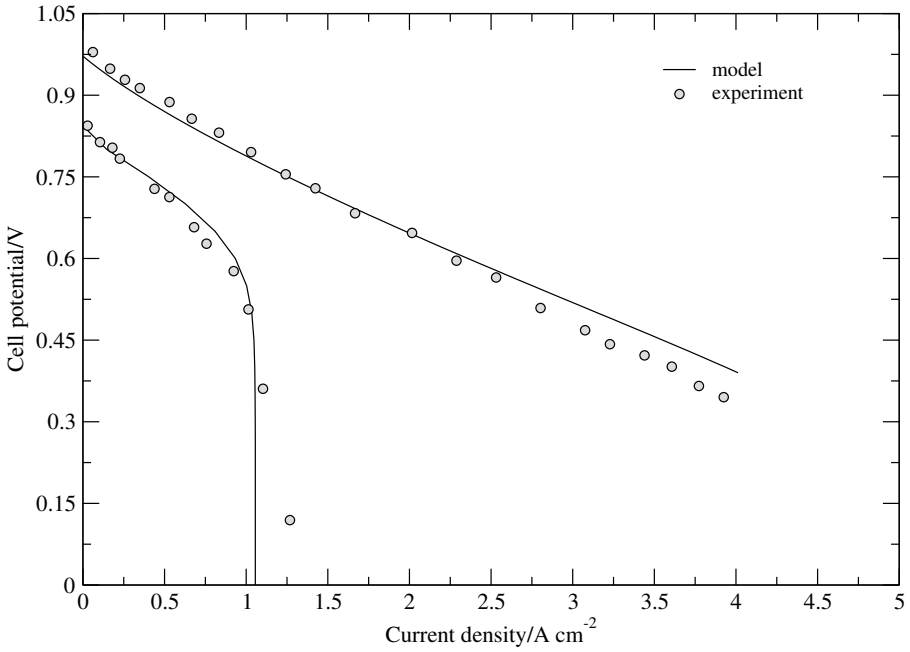

Figure 11: Comparison of model predictions with experimental [19] observation. Velocity of 5 m s^{-1} is used on the cathode as and the fuel inlet velocity is assumed to be 0.05 m s^{-1}. Operating temperature = 1073.15 K and Operating pressure = 100000 Pa.